Cellulose (2013) 20:2731–2744
DOI 10.1007/s10570-013-0072-7

ORIGINAL PAPER

# The swelling and dissolution of cellulose crystallites in subcritical and supercritical water

**Lasse K. Tolonen · Paavo A. Penttilä · Ritva Serimaa · Andrea Kruse · Herbert Sixta**

Received: 29 July 2013 / Accepted: 27 September 2013 / Published online: 10 October 2013


**Abstract** The swelling and dissolution phenomena of microcrystalline cellulose (MCC) were investigated in subcritical and supercritical water. Commercial MCC was treated in water at temperatures of 250–380 °C and a pressure of 250 bar for 0.25–0.75 s. As reaction products, undissolved but depolymerised cellulose residue, short-chain cellulose precipitate, water-soluble cello-oligosaccharides and monosaccharides, as well as their degradation products, were detected. The highest yield of the cellulose II precipitate was obtained after a reaction time of 0.25 s at 360 °C. Our hypothesis was that if the crystallites were swollen, the depolymerization pattern would be that of homogeneous reaction and the cellulose Iβ to cellulose II transformation would be observed. The changes in the structure of the undissolved cellulose residue were characterised by size exclusion chromatography, wide-angle X-ray scattering and $^{13}C$ solid-state NMR techniques. In many cases, the cellulose residue samples contained cellulose II; however, due to experimental limitations, it remains unclear whether it was formed through the swelling of crystallites or the partial readsorption of the dissolved cellulose fraction. The molar mass distributions of untreated MCC and after low intensity treatments showed a bimodal shape. After high intensity treatments the high molar mass chains disappeared which indicated a complete swelling or dissolution of the crystallites.

**Keywords** Subcritical water · Supercritical water · Microcrystalline cellulose · Cellulose precipitate · Cellulose dissolution

## Introduction

Current awareness of inevitably-dwindling fossil fuels along with concern about climate change has boosted

**Electronic supplementary material** The online version of this article (doi:10.1007/s10570-013-0072-7) contains supplementary material, which is available to authorized users.

L. K. Tolonen (✉) · H. Sixta
Department of Forest Products Technology, Aalto University, P.O. Box 16300, 00076 Espoo, Finland
e-mail: lasse.tolonen@aalto.fi

H. Sixta
e-mail: herbert.sixta@aalto.fi

P. A. Penttilä · R. Serimaa
Department of Physics, University of Helsinki, P.O. Box 64, 00014 Helsinki, Finland

A. Kruse
Institute of Agricultural Engineering, Conversion Technology and Life Cycle Assessment of Renewable Resources (440f), University of Hohenheim, P.O. Box, 70593 Stuttgart, Germany

A. Kruse
Institute for Catalysis Research and Technology, Karlsruhe Institute of Technology (KIT), P.O.Box 3640, 76021 Karlsruhe, Germany

research into alternative carbon sources. Photosynthesis converts $1.0 \times 10^{14}$ kg of carbon into biomass annually (Siegenthaler and Sarmiento 1993), and it has been estimated that about $1 \times 10^{20}$ J/a of primary energy can be produced from biomass in a sustainable manner (Parikka 2004). Thus, being renewable, carbon-neutral and abundantly available, biomass offers a credible alternative for replacing a significant part of fossil-based hydrocarbons. Using lignocellulosic biomass as fuel or platform chemicals requires a liquefaction or gasification process. Among many options, hydrothermal treatments via subcritical or supercritical water have gained momentum as promising processes for research and industry (Kruse 2008). As an example, subcritical water can be used for cellulose hydrolysis (Tolonen et al. 2011) and supercritical water for biomass gasification (Kruse 2008).

Cellulose, the main component in biomass, is characterised by its insolubility in water and most organic solvents. This sets large challenges for its dissolution or liquefaction. Although it is evident that cellulose is insoluble in ambient water, it was found in the 1990s that subcritical and supercritical water could hydrolyse crystalline cellulose without an added catalyst, converting cellulose to water-soluble reaction products (Bobleter et al. 1994; Sasaki et al. 1998). In the vicinity of the critical point of water, short-chain cellulose fractions dissolved and precipitated upon cooling (Ehara and Saka 2002; Sasaki et al. 2000), implying an increase in cellulose's solubility. Deguchi et al. (2008a, b) reported that cellulose crystallites underwent a crystalline-to-amorphous transition in subcritical water at around 300 °C, which is considered a prerequisite for polymer dissolution. A similar decrystallisation was not found in ethanol, revealing that the phenomenon was not a simple thermal decrystallisation, but a swelling phenomenon in which water played a significant role (Deguchi et al. 2006). The direct dissolution of cellulose as a polymer in subcritical or supercritical water is an appealing concept because it avoids the use of additional, environmentally-hazardous solvents and the investment in the associated recycling systems (Fink et al. 2001). To date, the reported yields and the degrees of polymerisation of the dissolved cellulose have been very moderate (Sasaki et al. 2003, 2004).

In this paper, we aim to confirm the swelling of cellulose crystallites and subsequent dissolution as a polymer. The paper describes a series of experiments in which commercial microcrystalline cellulose (MCC) was treated in subcritical and supercritical water. Our hypothesis is that if the crystallites were swollen, the depolymerization pattern in the undissolved residue particles would be that of a homogeneous depolymerisation reaction, and the cellulose Iβ to cellulose II transformation would be observed. Wide-angle X-ray scattering (WAXS) and $^{13}C$ solid-state NMR were used to study the changes in the cellulose crystallites' structure. Viscosity and size exclusion chromatography (SEC) methods were employed to investigate cellulose depolymerisation. The amounts of undissolved cellulose residue, cellulose precipitate and the total amount of water-soluble constituents were quantified.

## Experimental

A bench scale reactor system was constructed for the experiment (Fig. 1a). The system featured two feeding tanks, one for cellulose suspension and another for pure water. The cellulose suspension tank was equipped with a stirrer and an internal circulation pump. A high-pressure diagram pump (model Lewa EK3) with three pump heads featuring independently-adjustable stroke lengths was used to pump both water and cellulose suspension. All three lines were equipped with pulse dampers.

A cellulose suspension at room temperature was pumped from the cellulose feeding tank into the reactor, where it was instantaneously heated up to reaction temperature by mixing it with pre-heated supercritical water from the heating water line (Fig. 1b). The desired reaction temperature was maintained via heating elements around the reactor body, which eliminated heat losses. At the bottom of the reactor, the suspension was quenched down to 265 °C via quenching water and then subsequently lowered to room temperature via a cooler unit. The vertical down-flow reactor was made of high-alloy stainless steel (SAE designation type 4744) and had a volume of 390 µl. An air-loaded back-pressure regulator (Tescom 26-1721-24A) was used to control the pressure.

Commercial MCC was purchased from Merck (No. 1.02230.0500). The crystallinity of the MCC was 52 %, analyzed via WAXS as reported earlier (Tolonen et al. 2011). MCC was mixed with deionised

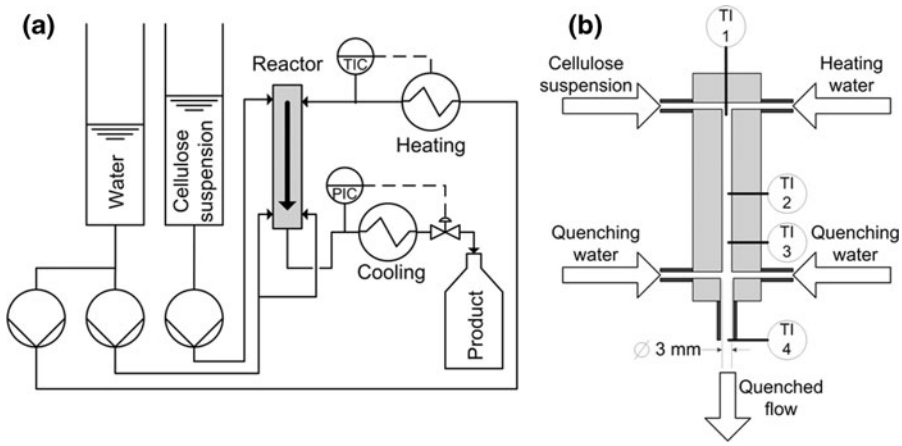


**Fig. 1** **a** Schematic of the reactor system, **b** the diagram of the reactor body and the locations of the thermocouples

water (conductivity below 1.0 μS/m). Prior to starting cellulose feeding, the system was preheated up to the reaction temperature using pure water. Cellulose suspension was poured into the cellulose feeding tank. The concentration in the feeding tank was 2.5 wt%. The reaction time ($t_{reaction}$) was controlled by setting the flow rates of heating water and cellulose suspension according to Eq. 1, where $V_{reactor}$ is the volume of the reactor part in $m^3$, $\dot{m}$ is the combined mass flow of cellulose suspension and heating water in kg/s and $\rho_{water}$ is the density of water at the reaction temperature and pressure in $kg/m^3$.

$$t_{reaction} = \frac{V_{reactor} \cdot \rho_{water}}{\dot{m}} \quad (1)$$

Reaction temperature was controlled by adjusting the temperature of the heating water flow according to an enthalpy balance and measured temperatures. The amount of quenching water needed to reach a desired post-quenching temperature was determined by the enthalpy balance calculations. In all calculations, cellulose suspensions were assumed to behave like pure water and to have perfect heat transfer. The densities and enthalpies of water as a function of temperature and pressure were obtained from a web database (Lemmon et al. 2013).

The reaction product was collected into a bottle at the reactor's outlet. The solid residue was separated from the liquid via two-stage filtration. First, most of the particles were filtered using a filter paper (S&S $589^2$), a Büchner-funnel and a vacuum pump. The filtered liquid was immediately re-filtrated using a 0.45 μm polyamide filter (Whatman No. 7404-044) to recover remaining solid particles. The non-dried solid cellulose residue cakes were extracted with acetone in a Soxhlet extractor for 18 h, in order to extract all hydrophobic substances that may have been formed in the reaction. The extracted samples were dried at room temperature to an equilibrium moisture content of about 96 % before being analysed.

The filtered liquid reaction products were stored at room temperature for 1 day to allow dissolved cellulose oligomers to precipitate. Thereafter, the liquid was concentrated via a rotary evaporator. When MCC was completely dissolved, the final concentration corresponded to 5 wt% of MCC; when part of the cellulose was removed as undissolved residue, the concentration was correspondingly lower. The concentrated solution was stored for 7 days at room temperature. The formed cellulose precipitate was separated by a 0.45 μm polyamide filter and dried at room temperature.

The yields of extracted cellulose residues and cellulose precipitate were determined gravimetrically. The total organic carbon (TOC) content of the liquid products was analysed by a Dimatoc 2,000 apparatus, and the results were converted to anhydroglucose equivalents ($m_{cellulose}=162/72 \cdot m_{TOC}$). The yield is reported as a percentage of the sum of the residue, precipitate and water-soluble products. The formation of gaseous products was assumed to be insignificant due to the short reaction times.

D-Glucose and D-fructose concentrations in water solutions were analysed via a UV photometrical sugar assay (r-biopharm 10139106035). Analysis of cello-oligosaccharides from DP2 to DP5 was performed using a high-performance anion exchange chromatography with pulsed amperometric detection. Before the

analysis, samples were diluted and filtered (0.45 μm). The components were separated using a CarboPac PA100 column set (guard and analytical). The solvents were composed of NaOH and $CH_3COONa$. Furanic compounds were analysed via ion chromatography (150983 LiChrospher® 100 RP-18, 5 μm) coupled with a UV–Vis detector (Hitachi L-7400) using 10 % aqueous acetonitrile as an eluent.

SEM-micrographs were taken using a scanning electron microscope (FE-SEM DSM 982 Gemini device by Zeiss) in backscatter electron mode at 10 keV beam energy. All the samples were coated by a few nanometers of Pt/Pd (Cressington Sputter Coater 208 HR) to prevent the nonconductive fibres being charged by beam electrons.

Viscosity-average degree of polymerisation was determined from the intrinsic viscosity measurement after dissolution in cupri ethylenediamine according to the SCAN-CM 15:99 method. The correlation $[\eta] = 0.42\ DP_v$ was used to calculate the degree of polymerisation from the viscosity values (Gruber and Gruber 1981). The molar mass distribution of the cellulose precipitate was analysed using a SEC-RI system calibrated by narrow pullulan standards after dissolution in LiCl/DMAc (Schelosky et al. 1999). The system comprised of PLgel Mixed-A 20 μm, (50 × 7.5 mm) and 4 × (300 × 7.5 mm) columns, and a Shodex RI-101 RI-detector. A flow rate of 0.750 ml/min and a temperature of 25 °C were used. For each sample, double injections were used with an injection volume of 150 μl. The molar mass distribution of the cellulose residue was analysed using a SEC-MALLS/RI-system (Wyatt DAWN DSP) with a similar column setup and run parameters. Due to MALLS-detector's insensitivity for low molar mass polymers, the linear part of the calibration curve was linearly extrapolated to the low molar mass region in the calculation of the molar mass distributions. The deconvolution of the molar mass distribution curves of residue samples was done using Matlab's *curve fit* toolbox, as reported by Tolonen et al. (2011). A length of 5.2 Å for one monomer unit was used to convert a DP to the length of the crystallite (Baker et al. 1998).

The WAXS measurements were carried out with a laboratory setup ($\lambda = 1.54$ Å) as described earlier (Penttilä et al. 2010; Tolonen et al. 2011). The relative amount of cellulose II in the samples was estimated as a combination of three different methods: (1) the area below the 1–10 peak of cellulose II ($2\theta = 12.2°$) (Langan et al. 2005), (2) the ratio of the area below a calculated 4-peak WAXS intensity curve of cellulose II and below the measured intensity on 2θ range 10–25° and (3) a scaling coefficient used to multiply the measured intensity of a sample containing mostly cellulose II (0.25 s, 380 °C) when it was used to remove the contribution of cellulose II by subtraction. In the two latter methods, the scaling parameters were chosen so that the WAXS intensity resulting from the subtraction was as characteristic of the cellulose Iβ intensity as possible. The relative amount of cellulose II for the sample with the highest cellulose II content with all methods (0.75 s, 320 °C) was chosen as 0.9, and the corresponding values were calculated for all samples as the average of the results from the three different methods. The resulting values are thus not absolute, but should be suitable for comparison between different samples.

The width of the cellulose Iβ crystallites was estimated using the 200 reflection ($2\theta = 22.7°$). A fit with a linear background, a parabola on the top and two straight lines on the sides of the peak were used to gain the peak position and full width at half maximum. The corresponding crystal dimension was calculated using the Scherrer equation. To determine the width of cellulose Iβ crystallites in samples containing also the cellulose II polymorph, the contribution of cellulose II was removed from the measured WAXS intensity by subtracting the scaled intensity of a sample containing mostly cellulose II (0.25 s, 380 °C).

A $^{13}C$ CP-MAS NMR method was used for the structural analysis of cellulose residue. The method analysis was carried out as described by Zuckerstätter et al. (2009). The deconvolution of NMR-results was done according to Larsson, Wickholm and Iversen (Larsson et al. 1997; Wickholm et al. 1998).

## Results and discussion

### Reactor

The key operation parameters of the reactor are given in Table 1. Since the density and enthalpy of water vary widely as a function of pressure and temperature, all the feeding flows and the temperatures must be adjusted when one reaction parameter is changed.

The practical experience gained regarding the reactor operation merits some comment. We realised

**Table 1** Reactor operating parameters at a pressure of 25 MPa

| Time (s) | Temperature (°C) | | Flow (g/h) | | | Reynolds number |
|---|---|---|---|---|---|---|
| | Heating water | Reactor | Cellulose | Heating water | Quenching | |
| 0.25 | 388 | 320 | 1,575 | 2,363 | 1,063 | 5,500 |
| 0.25 | 395 | 340 | 1,467 | 2,201 | 1,430 | 5,623 |
| 0.25 | 417 | 360 | 1,320 | 1,979 | 1,732 | 5,713 |
| 0.25 | 493 | 380 | 1,010 | 1,514 | 1,904 | 5,679 |
| 0.50 | 385 | 300 | 832 | 1,248 | 354 | 2,675 |
| 0.50 | 388 | 320 | 788 | 1,181 | 532 | 2,750 |
| 0.50 | 395 | 340 | 734 | 1,100 | 715 | 2,811 |
| 0.50 | 417 | 360 | 660 | 990 | 866 | 2,857 |
| 0.50 | 493 | 380 | 550 | 757 | 953 | 2,840 |
| 0.75 | 381 | 280 | 580 | 870 | 101 | 1,725 |
| 0.75 | 385 | 300 | 555 | 832 | 236 | 1,784 |
| 0.75 | 388 | 320 | 525 | 788 | 354 | 1,830 |
| 0.75 | 395 | 340 | 489 | 734 | 477 | 1,874 |
| 0.75 | 417 | 360 | 440 | 660 | 577 | 1,904 |

that the perfect stability of flows was of great importance in avoiding temperature fluctuation in the mixing zone, which caused high stress to joints. It was also difficult to achieve an even temperature profile when the reactor was constructed from a single metal piece. This is due to the heat conduction from the joints of cold water lines, which could not be completely compensated by heating elements. In the experiments, the reaction temperature was measured by the thermocouple 2 (Fig. 1). In the lower part of the reactor, heat conduction caused a 20–30 °C drop in temperature from thermocouple 2 to thermocouple 3. We assumed constant hydrodynamic conditions and perfect plug-flow, although the Reynolds number varied. Because the solubility of atmospheric gases increases with temperature and pressure, accumulation of air inside the reactor was unlikely (Japas and Franck 1985).

The reaction temperature influenced not only the density but also the ion product and the static dielectric constant (Table 2). The dielectric constant decreased with the temperature, decreasing below 20 at the used temperatures, thus being below that of acetone at room temperature. At the applied reaction temperatures, the ion product decreased as the reaction temperature increased, thereby reducing the $H^+$ concentration; this affected the extent of the cellulose hydrolysis. At all applied reaction temperatures, the ion product inside the reaction zone was higher than at room temperature, giving a higher $H^+$ concentration compared with that in ambient water (Lemmon et al. 2013; Marshall and Franck 1981; Uematsu and Franck 1980). The ion product of the supercritical heating water was substantially lower.

## Reaction products

The experiments were carried out at temperatures from subcritical 280 °C to supercritical 380 °C for 0.25, 0.50 and 0.75 s, while the pressure was kept constant at 25.0 MPa. Subcritical and supercritical water treatment resulted in the rapid dissolution of MCC particles and the formation of various reaction products (Table 3). Below the *undissolved residue* is the solid fraction that was collected by filtration immediately after the treatment. *Cellulose precipitate* is the fraction that precipitated after the treatment and subsequent concentration. The rest of the reaction products remained water-soluble. These products contained *cello-oligosaccharides*, which are short cellulose chains remaining water-soluble at room temperature, as well as glucose, fructose, 5-hydroxymethylfurfural and furfural.

As expected, the amount of undissolved residue decreased with reaction time and temperature. The observed reaction rates confirm the earlier results that MCC is dissolved in a fraction of a second (Sasaki

**Table 2** Properties of water at 25 MPa based on literature values

| Temperature (°C) | Density (g/ml)[a] | | $Log_{10}$ (ion product)[b] | | Dielectric constant[c] | |
|---|---|---|---|---|---|---|
| | Heating water | Reactor | Heating water | Reactor | Heating water | Reactor |
| 25 | 1.01 | 1.01 | −13.9 | −13.9 | 79.4 | 79.4 |
| 280 | 0.43 | 0.78 | −14.7 | −11.1 | 9.5 | 20.0 |
| 300 | 0.31 | 0.74 | −16.5 | −11.1 | 5.8 | 18.2 |
| 320 | 0.24 | 0.70 | −18.0 | −11.3 | 3.9 | 16.3 |
| 340 | 0.18 | 0.66 | −19.4 | −11.6 | 2.8 | 14.3 |
| 360 | 0.13 | 0.59 | −21.1 | −12.1 | 2.1 | 12.0 |
| 380 | 0.09 | 0.45 | −23.2 | −13.5 | 1.6 | 8.2 |

Heating water: the preheated water from preheater into the reactor. Reactor: the conditions in the reaction zone

[a] Lemmon et al. (2013)

[b] Marshall and Franck (1981)

[c] Uematsu and Franck (1980)

**Table 3** The yields of different quantified constituents after subcritical or supercritical water treatment

| Time (s) | Temperature (°C) | Residue (%) | Precipitate (%) | COS2–5 (%) | Glucose (%) | Fructose (%) | 5-HMF (%) | Furfural (%) |
|---|---|---|---|---|---|---|---|---|
| 0.25 | 320 | 63 | 0 | 13 | 4 | 0 | 0 | 0 |
| 0.25 | 340 | 58 | 5 | 16 | 2 | 1 | 0 | 0 |
| 0.25 | 360 | 46 | 24 | 19 | 2 | 0 | 0 | 0 |
| 0.25 | 380 | 27 | 23 | 25 | 3 | 1 | 1 | 0 |
| 0.50 | 300 | 71 | 7 | n.d. | 2 | 0 | 0 | 0 |
| 0.50 | 320 | 53 | 14 | n.d. | 7 | 1 | 0 | 0 |
| 0.50 | 340 | 33 | 8 | n.d. | 10 | 2 | 0 | 0 |
| 0.50 | 360 | 0 | 15 | n.d. | 18 | 4 | 1 | 0 |
| 0.50 | 380 | 0 | 5 | n.d. | 13 | 4 | 1 | 0 |
| 0.75 | 280 | 54 | 3 | n.d. | 9 | 2 | 0 | 0 |
| 0.75 | 300 | 39 | 9 | n.d. | 9 | 0 | 0 | 0 |
| 0.75 | 320 | 29 | 12 | n.d. | 5 | 1 | 1 | 0 |
| 0.75 | 340 | 0 | 8 | n.d. | 5 | 2 | 2 | 1 |
| 0.75 | 360 | 0 | 3 | n.d. | 4 | 1 | 5 | 2 |

*COS* cello-oligosaccharides

et al. 2000, 2004). For example, at a reactor temperature of 380 °C, 73 % of MCC was dissolved in 0.25 s. Cellulose precipitate was formed 0–24 wt% of initial MCC. The maximum yield was achieved using a 0.25 s reaction time and 360 °C. With longer reaction times, the maximum yield of the cellulose precipitate decreased as the dissolved cellulose chains were degraded. The yield of the cellulose precipitate reached its maximum near the temperature where the complete dissolution of MCC was achieved. The amounts of water-soluble cello-oligosaccharides were analysed for the 0.25 s series. The amount of cello-oligosaccharides increased with the temperature. An increasing temperature and extended reaction time produced increasing amounts of 5-HMF and furfural. It is estimated that a substantial part of the unidentified constituents was present in the form of cello-oligosaccharides and various organic acids, as previously reported in the literature (Ehara and Saka 2002; Kabyemela et al. 1999).

A clear distinction between the cellulose the precipitate and the residue fractions is important, but we found it problematic to separate dissolved reaction products from the solid cellulose residue using filtration. The formed residue consisted of very small particles, which slowed down the filtration rate. Fast separation is essential because dissolved cellulose polymers easily adsorb onto the residue particles (Yu and Wu 2009). Since our filtration procedure took 15–90 min, it is probable that the adsorption of cellulose precipitate occurred to some extent in the experiments. In this case, the actual amounts of cellulose residue and precipitate would be lower and higher, respectively, as listed in Table 3. However, the influence on the concentration of the water-soluble product would be insignificant. Fast precipitation is an intrinsic problem that cannot be completely avoided. The separation of the precipitate from the residue cannot be done before the temperature is reduced by cooling, which allows the precipitation to occur if the precipitation of the high molar mass cellulose chains is fast. An alternative way to reduce the amount of precipitate in the residue would be to degrade the dissolved cellulose chains at a high temperature.

Sasaki et al. (2000) reported that the rate of dissolution increased near the critical point, hypothesising that the cellulose crystallites swelled and finally dissolved under those conditions. Our results confirm that the cellulose chain's solubility was increased because a cellulose precipitate that is insoluble in ambient water was formed. The precipitate was formed under both subcritical and supercritical conditions. This observation is supported by Yu and Wu (2009), who reported the dissolution of the chains up to a degree of polymerisation (DP) of 25–30 at 280 °C and 20 MPa, as well as by Deguchi et al. (2008a, b), who reported decrystallisation at 300 °C. These results indicate that the dissolution does not occur at the critical point, but that it is gradually promoted via increasing temperature.

There are many factors that possibly contribute to water's capability to dissolve crystalline cellulose. Many solvent properties are already significantly shifted in subcritical water, compared with those of ambient water. For instance, the water's continuous hydrogen bond network ceases at 200 °C (Blumberg et al. 1984; Kalinichev 2001). When the temperature is raised, the dielectric constant of water decreases; it starts to resemble more nonpolar organic solvents and its ability to solvate hydrophobic top and bottom faces of cellulose chains increases. This presumably facilitates dissolution because these intersheet forces are suggested to be the main cause of the insolubility of cellulose in most solvents (Gross et al. 2012). It must be remembered, however, that cellulose is not soluble in non-polar organic solvents, such as acetone. Also, water remains a polar molecule in the supercritical state and only its macroscopic ability to adjust the electric field is changed, which is measured as a change in the dielectric constant. Therefore, the cellulose's solubility in supercritical water is not determined by dielectric constant alone, and it must be related also to the other properties of near- and supercritical-water.

## Crystal structure

WAXS was used to analyse the width of cellulose Iβ crystallites and the relative abundance of the polymorphs Iβ and II (Fig. 2; Table 4). All WAXS-intensity curves are available as electronic supplementary information (ESI). The treatment changed the structure of the cellulose crystallites in the residue samples. The measured WAXS intensities of most of the extracted cellulose residues resembled the so-called cellulose $IV_I$ crystal structure, which in light of recent findings appears to be the same as cellulose Iβ but with extraordinarily shaped crystals, leading to an overlapping of the 1–10 and 110 reflections (Newman 2008). This interpretation has been adopted in the following discussion and the structure is referred to as cellulose Iβ instead of $IV_I$. Also, cellulose II polymorph was identified in many of the residue samples. As a trend, the cellulose II peak at 12.2° was more intense at higher treatment intensities, whereas no cellulose II peak was found at low treatment intensities. Formation of cellulose II did not require supercritical temperatures, but was already formed e.g. at 300 °C and 0.75 s. The 004 peak of cellulose Iβ was observed to gradually disappear as conversion increased. This may imply the average shortening of the crystallites, or that the long-distance order in the longitudinal direction of the cellulose chains decreased. In general, the treatment increased the width of the Iβ crystallites in the cellulose residues, as determined from the 200 reflection (after subtracting the contribution of cellulose II, if needed). The WAXS analysis of the precipitate from the experiment at

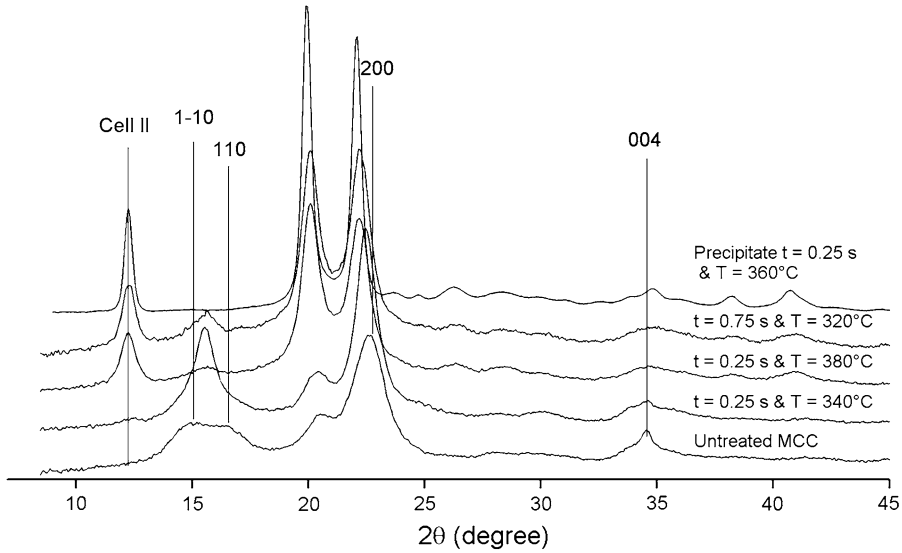


**Fig. 2** The wide-angle X-ray scattering intensities of untreated MCC, selected treated residues and one cellulose precipitate sample. All wide-angle X-ray scattering data is available as ESI. The locations of the reflections of cellulose Iβ and the cellulose II peak are marked in the figure

**Table 4** WAXS and $^{13}C$ solid-state NMR data of the residue samples

| Time (s) | Temperature (°C) | X (%) | WAXS | | NMR | |
|---|---|---|---|---|---|---|
| | | | Cell II (%) | CrW (nm) | CRI (%) | FibrilW (nm) |
| – | – | 0 | 0 | 5.2 | 54.1 | 4.3 |
| 0.25 | 320 | 63 | 0 | 7.7 | n.d. | n.d. |
| 0.25 | 340 | 58 | 4.1 | 8.5 | 41.1 | 3.2 |
| 0.25 | 360 | 46 | 12 | 9.5 | n.d. | n.d. |
| 0.25 | 380 | 27 | 80 | n.d. | 68.7 | 8.3 |
| 0.50 | 300 | 71 | 5.3 | 8.7 | 40.9 | 3.2 |
| 0.50 | 320 | 53 | 24 | 9.1 | n.d. | n.d. |
| 0.50 | 340 | 33 | 68 | 7.6 | n.d. | n.d. |
| 0.75 | 280 | 54 | 0 | 7.3 | n.d. | n.d. |
| 0.75 | 300 | 39 | 28 | 7.4 | n.d. | n.d. |
| 0.75 | 320 | 29 | 90 | n.d. | n.d. | n.d. |

X: yield of undissolved residue, Cell II: cellulose II content, CrW: crystallite width of cellulose Iβ crystallites, CRI: crystallinity index, FibrilW: fibril width

360 °C for 0.25 s indicated that the cellulose precipitate had highly crystalline cellulose II polymorph with large crystallites.

The treatment drastically changed the NMR-spectra (Fig. 3). The spectra of treated samples showed significant noise, making it difficult to deduct the crystallinity values and the fibril dimensions (Table 4). Qualitatively, the disappearance of the peaks associated with accessible fibril surfaces at 82–85 ppm indicated the fusion of the elementary fibrils in supercritical water (t = 0.25 s and T = 380 °C in Fig. 3) (Wickholm et al. 1998), or merely the transformation from cellulose Iβ to cellulose II. The samples treated under milder conditions (e.g. t = 0.25 s and T = 340 °C in Fig. 3) still exhibited those peaks assigned for fibril surfaces after the treatment. The formation of cellulose II in the residue samples was confirmed by the appearance of the cellulose II peak at 105.9 ppm in the C1 region (Larsson et al. 1997). The NMR-spectrum of a high-intensity treated sample (t = 0.25 s and T = 380 °C) closely resembled that of the cellulose precipitate from the same experiments (Precipitate of the sample t = 0.25 s and T = 380 °C in Fig. 3). The precipitate shows an exceptionally clear pattern of highly crystalline cellulose II.

The results of the WAXS and NMR analyses both confirm the formation of cellulose II in the cellulose residue samples. Its amount increased substantially when the residue's yield decreased below 60 %. A very similar trend was reported by Sasaki et al. (2004). The appearance of the cellulose II polymorph can be explained by two mechanisms. The first mechanism is the swelling and rearrangement of the cellulose chains without dissolution. The second mechanism is the molecular dissolution and adsorption of dissolved cellulose chains onto crystallites upon cooling. Reaction temperature alone did not explain the formation of the cellulose II peak, but the onset temperature varied depending on the reaction time. Therefore, temperature

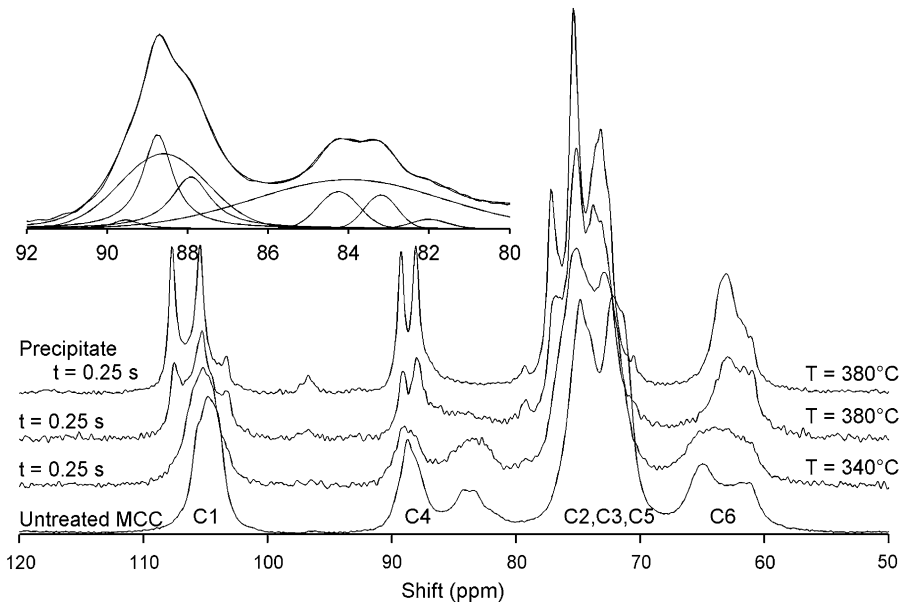


**Fig. 3** NMR-spectra of selected samples. The deconvolution of the C4 region of the untreated MCC sample is presented in the insert. All NMR data is available as ESI

alone does not trigger the transformation from cellulose Iβ to cellulose II; instead, it appears to require other changes in the cellulose structure, like the loosening of the fibrillar structure through depolymerisation. The role depolymerisation plays was reported by Deguchi et al. (2008b), who showed that the depolymerisation and disappearance of the cellulose crystallites were facilitated by adding $H_2SO_4$ as a catalyst. The hypothesised relaxation of the fibrillar structure may also enable the fusion of the crystallites, which was seen in the increased crystallite dimensions. The cellulose precipitate samples in turn showed pure cellulose II polymorph, which is strong evidence for real dissolution as a molecular solution and not as cellulose I aggregates.

## SEM-micrographs

Scanning electron microscope micrographs (Fig. 4) show how the MCC particles were radically changed and the initial shape of the particles was quickly lost in the treatment. The average length of untreated cellulose particles was estimated to be 20 μm. In low-intensity treatments, the particles retained their original shape (e.g. t = 0.25 s, T = 32 °C). After high-intensity treatments, the particles were mostly disintegrated to fragments with diameters of less than one micrometer (e.g. t = 0.25 s, T = 380 °C; t = 0.75 s, T = 320 °C). When MCC was treated in subcritical water in our previous study, such severe disintegration was not observed (Tolonen et al. 2011). The reorganisation and aggregation of the remaining particles was evident in high-intensity experiments; the sample t = 0.75 s and T = 320 °C in particular exhibited large aggregates. The appearance of the high-intensity treated samples closely resembled that of the cellulose precipitate published earlier (Yu and Wu 2009). This indicates the possible adsorption of the cellulose precipitate onto the residue particles. Small granulate-looking particles, probably precipitated cellulose deposited on the MCC particles, are visible in a low-intensity sample (t = 0.25 s and T = 320 °C) and in an increased amount in a sample with a longer reaction time (t = 0.50 s and T = 320 °C). Noteworthy is that a sample may be largely disintegrated and still contain only a minor amount of cellulose II, as in the sample t = 0.25 s and T = 360 °C.

## Degree of polymerisation

Near- and supercritical-water treatment severely depolymerised the cellulose chains in the cellulose residue, which was observed as a reduction in the viscosity-average degree of polymerisation (Fig. 5). The viscosity of the residue samples decreased as the reaction intensity increased. A similar linearly-decreasing trend to very low DP values was published

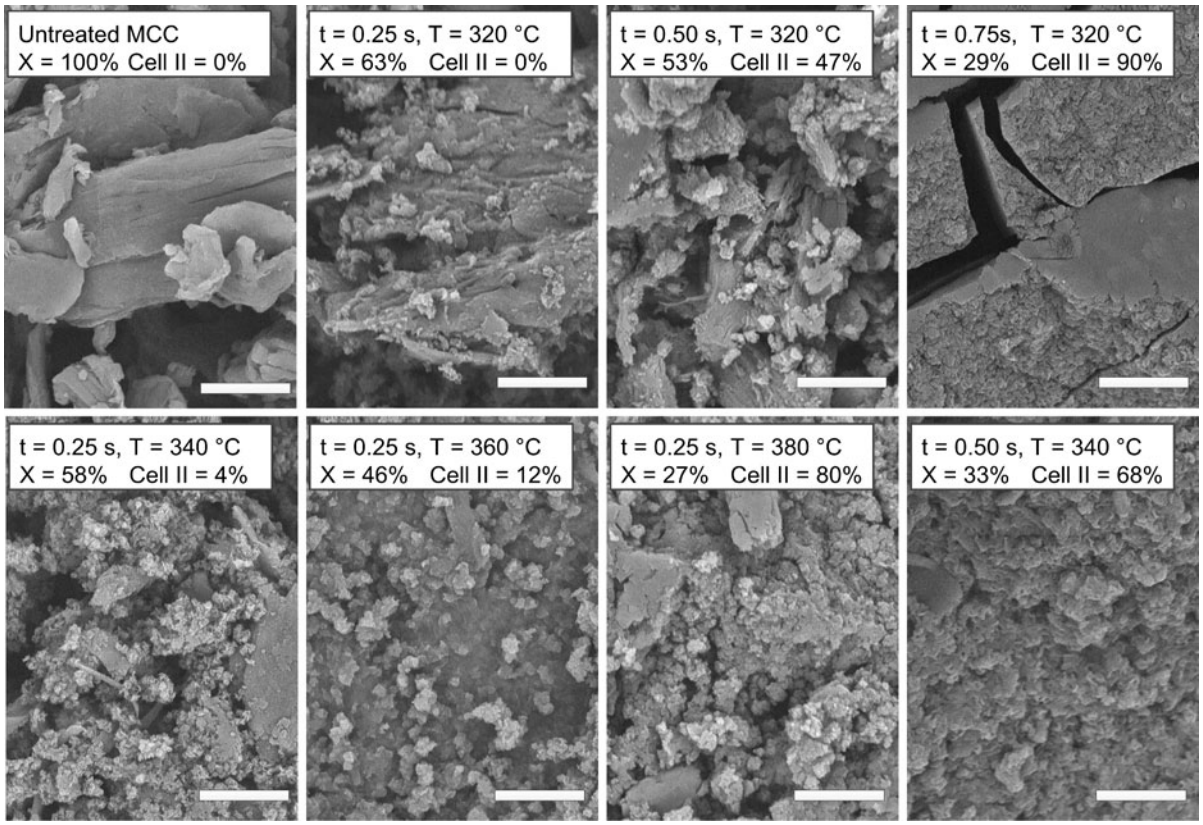


**Fig. 4** The SEM-micrographs of undissolved cellulose residue particles after acetone extraction. Applied reaction time (t), temperature (T), Yield of undissolved residue (X), and cellulose II determined by WAXS (Cell II) are shown in the figures. *Scale bar* 5.0 μm

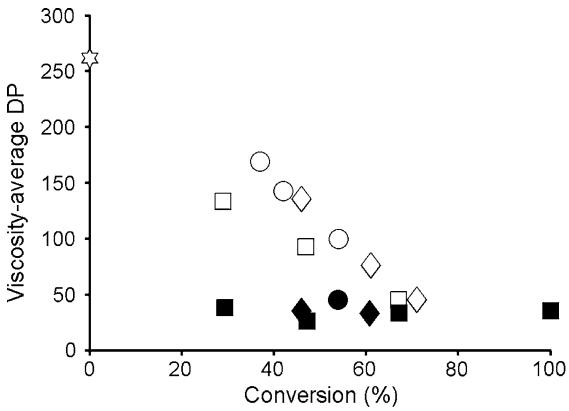


**Fig. 5** Viscosity average degree of polymerisation vs. degree of conversion (100 %—yield of undissolved residue %) *star* Reference, *circle* 0.25 s, *square box* 0.50 s, *diamond* 0.75 s. *White symbol* residue sample. *Black symbol*: precipitate sample

earlier by Sasaki et al. (2004). When the amount of recovered precipitate allowed, its DP was also analysed. The cellulose precipitate had a low viscosity-average DP, between 11 and 19 anhydroglucose units. The DP of the precipitate was not noticeably affected by the applied reaction conditions.

Interestingly, no level-off degree of polymerisation (LODP) was found, but a very low viscosity-average DP of 45 resulted as treatment intensity increased. The LODP is a characteristic feature of crystalline cellulose under non-swelling reaction conditions, as cellulose Iβ values are typically above a DP of 100 (Battista et al. 1956). The absence of an LODP distinguishes these results from our previous experiments in subcritical water, in which a clear LODP around DP160 was found for the same MCC. The LODP held even when less than 30 % of the initial cellulose remained after the treatment (Tolonen et al. 2011). Although counterintuitive, the LODP behavior does not mean that no depolymerisation or dissolution took place. This can be explained by assuming that the reactive domains were randomly distributed and that the dissolution of the crystallites was restricted to their

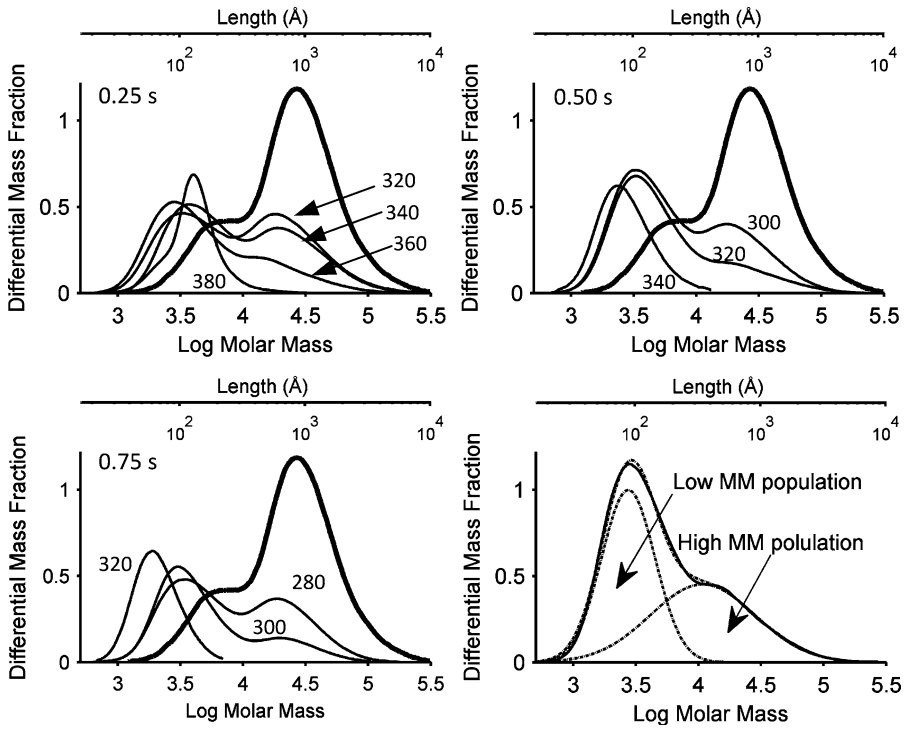


**Fig. 6** Molar mass distributions of extracted cellulose residues multiplied by the corresponding yield, and an example of the deconvolution of the low and high MM populations for the sample treated at 360 °C for 0.25 s. The reaction time and temperature as °C are shown in the figure. The upper axes show the corresponding lengths of the linear chains. Thick solid line: untreated MCC. *Thin solid line* treated sample. Deconvolutions of all the MMDs are available as ESI

**Table 5** Extracted deconvolution parameters of molar mass distributions of acetone-extracted cellulose residues

| Time (s) | Temperature (°C) | X (%) | $A_{low}$ | $A_{high}$ | $\mu_{low}$ (DP) | $\mu_{high}$ (DP) | Cell II (%) |
|---|---|---|---|---|---|---|---|
| – | – | 0 | 0.17 | 0.82 | 32 | 174 | 0 |
| 0.25 | 320 | 63 | 0.25 | 0.38 | 19 | 116 | 0 |
| 0.25 | 340 | 58 | 0.26 | 0.33 | 22 | 121 | 4 |
| 0.25 | 360 | 46 | 0.25 | 0.22 | 17 | 67 | 12 |
| 0.25 | 380 | 27 | 0.09 | 0.18 | 25 | 24 | 80 |
| 0.50 | 300 | 71 | 0.37 | 0.35 | 20 | 106 | 5 |
| 0.50 | 320 | 53 | 0.33 | 0.20 | 20 | 81 | 24 |
| 0.50 | 340 | 33 | 0.17 | 0.16 | 13 | 21 | 68 |
| 0.75 | 280 | 54 | 0.27 | 0.28 | 21 | 117 | 0 |
| 0.75 | 300 | 39 | 0.27 | 0.13 | 19 | 95 | 28 |
| 0.75 | 320 | 29 | 0.29 | 0.00 | 12 | n.d. | 90 |

X: the yield of undissolved residue. $A_{low}$ and $A_{high}$ indicate the size of low and high molar mass population, respectively. $\mu_{low}$ (DP) and $\mu_{high}$ (DP) indicate the peak position of the Gaussian fit as DP. Cell II indicates the amount of cellulose II in the sample, estimated by WAXS

ends, which causes the unchanged DP of the residue upon a progressing depolymerization (Sharples 1957, 1958). Inversely, the absence of the LODP, which was observed in this study, can be interpreted as an indication of the crystallite swelling. However, a similar trend in the LODP behavior would be obtained if short dissolved chains precipitated on the crystallites.

SEC was used to elucidate the depolymerisation behavior. Untreated MCC and moderately-treated residues exhibited a bimodal shape of MMD (Fig. 6). As the treatment intensity and the degree of

conversion increased, the shapes of the MMDs shifted toward unimodal distribution and a lower molar mass. The MMDs were deconvoluted into two Gaussian-shaped populations named 'low' and 'high' according to their molar masses (Fig. 6). The obtained deconvolution results are tabulated in Table 5. All molar mass distributions and deconvolutions are provided as ESI.

As a trend, the high molar mass (MM) population ($A_{high}$) was reduced in the treatment, and the population of low molar mass polymers ($A_{low}$) increased in relation to $A_{high}$. The low molar mass population also increased in absolute size, and not just in relation to the high molar mass population. This suggests that high molar mass polymers were depolymerised prior to dissolution, thus growing the low molar mass population. The mass of the high molar mass population, $A_{high}$, decreased almost linearly with the yield of the undissolved residue, reaching zero when approximately 75 % of the initial amount of MCC was dissolved. Equal to the viscosity analysis, the depolymerisation followed the same pattern with different reaction times.

Bimodal MMDs have been reported in the literature for extensively degraded cellulose samples at their LODP (Isogai et al. 2009; Tolonen et al. 2011). Here, the bimodality must not be confused with the bimodal shape commonly found in hemicellulose-containing pulps. The bimodal form of MMDs is interesting because random depolymerisation does not produce a bimodal MMD, but a unimodal Flory–Schultz distribution. Implicitly, this means that the depolymerisation reactivity of cellulose chains is heterogeneous when a bimodal shape is generated.

We hypothesise that the cellulose crystallites consist of two types of domains: reactive chains on the surfaces (particularly at the ends of the crystallites), and core chains covered by the reactive surface chains (Fig. 7). These protected core chains are the high molar mass population in the MMDs. This is in agreement with the observation that the DP of the high MM population decreases linearly against the decreasing yield and the DP of the residue, indicating that protected core chains are not subjected to the random scission of the chains; instead, the degradation is restricted to the ends of the crystallites. The disappearance of the distinguishable high MM population at 380, 340 and 320 °C after a treatment for 0.25, 0.50 and 0.75 s, respectively, suggests that the high

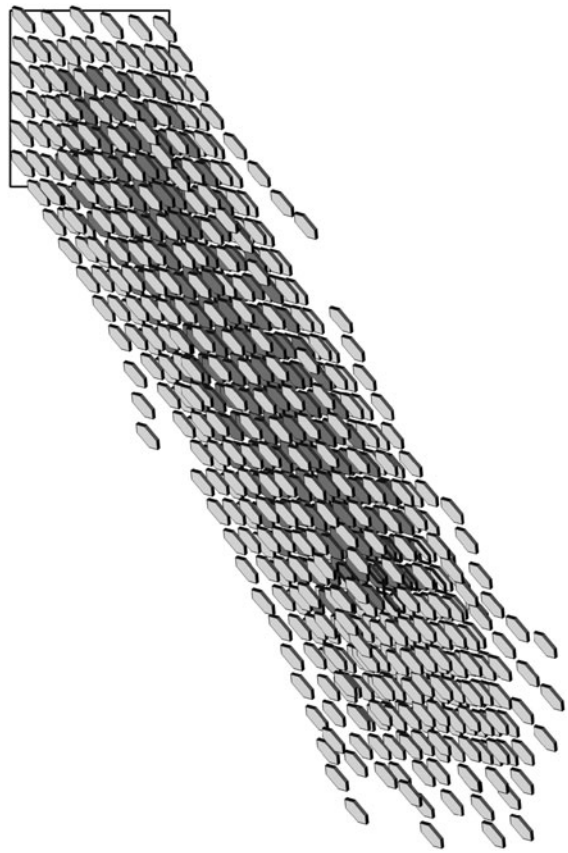

**Fig. 7** Illustration showing the locations of the surface chains (*light gray*) and protected core chains (*dark gray*) at one end of a cellulose crystallite

reaction intensities caused the destruction of the core crystallites. The core chains are here defined merely by their accessibility. This definition does not require that the core domains are perfectly crystalline, which explains why substantially shorter crystallite lengths have been reported in the chain direction (Leppänen et al. 2009).

The accessible and therefore more reactive surface chains form the low molar mass population. We noticed that the share of the reactive chains increased with the reaction intensity. This may be the result of an increasing swelling depth of the surface layer, as suggested earlier (Sasaki et al. 2004), or merely the result of the adsorption of the dissolved chains back onto the surfaces. Because the molar mass of the low MM fraction is close to that of the cellulose precipitate, it is impossible to distinguish these two mechanisms based on the present results. Nonetheless, it is safe to say that the low MM population is not produced

merely by adsorption only because the low MM population is found in the untreated MCC and in some of the treated samples containing little or no cellulose II (e.g. t = 0.25 s and T = 360 °C).

## Conclusions

We investigated the possibility of decrystallising and dissolving cellulose in subcritical and supercritical water while retaining its polymeric structure. MCC powder was treated at 250–380 °C for 0.25–0.75 s. In agreement with earlier published papers (Ehara and Saka 2002; Sasaki et al. 2004), MCC was dissolved as a mixture of low molar mass cellulose, monosaccharides and their degradation products. Part of the polymeric cellulose that was dissolved precipitated after the treatment, forming highly crystalline but low molar mass cellulose II. The existence of the cellulose precipitate confirmed the earlier reported increased solubility of cellulose in subcritical and supercritical water (Ehara and Saka 2002; Sasaki et al. 2004). This study suggests that polymeric dissolution occurs at around 300 °C. The increasing temperature promotes the dissolution, but requires that the reaction time is kept short in order to prevent the degradation of the dissolved cellulose chains.

A combination of WAXS, GPC, and NMR techniques was employed in order to gain new experimental evidence of the decrystallisation and swelling of the crystallites. We hypothesised that if the crystallites were swollen or dissolved, the cellulose chains concealed inside the crystallites would be depolymerised whereas in the opposite case without swelling, the normal LODP pattern would be observed. Swelling or dissolution would also enable the transformation of cellulose Iβ to thermodynamically more stable cellulose II form.

The results from the present work showed that the undissolved cellulose residue samples contained cellulose II polymorph, which may be a result of swelling and rearrangement of the cellulose chains. Very low DP values were detected from the undissolved cellulose residue samples. This absence of the normal LODP suggests the swelling of the crystallites, because the chains are not protected from chain scission by their crystalline structure. These results indicates that the initial cellulose crystallites were destructed in the high intensity treatments. It is more difficult, however, to conclude if the mere swelling without dissolution occurred in any of the experiments. The fast precipitation and readsorption of the dissolved chains onto the crystallites before being separated by filtration undoubtedly contributed, at least partially, to the presence of cellulose II and the low DP chains in the residue samples. Therefore, the fast separation of the solid residue from the dissolved chains is essential, which poses a major experimental challenge. As long as this cannot be done, it is not possible to definitively distinguish between the dissolution-adsorption and swelling mechanisms.

**Acknowledgments** We would like to acknowledge Berkan Aksoy for his diligent laboratory work; Thomas Tietz and Matthias Pagel for their work on the reactor and Caroline Vanderghem, Gerhard Zuckerstätter, Wilhelm Habicht, Walter Milacher, Armin Lautenbach and Birgit Rolli for their great help with analyses. We gratefully acknowledge the Future Biorefinery Program within Finnish Bioeconomy Cluster Ltd and the Finnish Funding Agency for Technology and Innovations (TEKES) for funding this research.

## References

Baker AA, Helbert W, Sugiyama J, Miles MJ (1998) Surface structure of native cellulose microcrystals by AFM. Appl Phys A 66:S559–S563. doi:10.1007/s003399870002

Battista OA, Coppick S, Howsmon JA, Morehead FF, Sisson WA (1956) Level-off degree of polymerization. Ind Eng Chem 48:333–335. doi:10.1021/ie50554a046

Blumberg RL, Stanley HE, Geiger A, Mausbach P (1984) Connectivity of hydrogen bonds in liquid water. J Chem Phys 80:5230–5241. doi:10.1063/1.446593

Bobleter O, Grif M, Huber C (1994) Thermal hydrolysis of plant materials with water and alkaline solutions. Ger Offen 5

Deguchi S, Tsujii K, Horikoshi K (2006) Cooking cellulose in hot and compressed water. Chem Commun 31:3293–3295. doi:10.1039/B605812D

Deguchi S, Tsujii K, Horikoshi K (2008a) Crystalline-to-amorphous transformation of cellulose in hot and compressed water and its implications for hydrothermal conversion. Green Chem 10:191–196. doi:10.1039/B713655B

Deguchi S, Tsujii K, Horikoshi K (2008b) Effect of acid catalyst on structural transformation and hydrolysis of cellulose in hydrothermal conditions. Green Chem 10:623–626. doi:10.1039/B803384F

Ehara K, Saka S (2002) A comparative study on chemical conversion of cellulose between the batch-type and flow-type systems in supercritical water. Cellulose 9:301–311. doi:10.1023/A:1021192711007

Fink H, Weigel P, Purz HJ, Ganster J (2001) Structure formation of regenerated cellulose materials from NMMO-solutions. Prog Polym Sci 26:1473–1524. doi:10.1016/S0079-6700(01)00025-9

Gross AS, Bell AT, Chu J (2012) Entropy of cellulose dissolution in water and in the ionic liquid 1-butyl-3-

methylimidazolim chloride. Phys Chem Chem Phys 14:8425–8430. doi:10.1039/C2CP40417F

Gruber E, Gruber R (1981) Viskosimetrische bestimmung des polymerisationsgrades von cellulose. Papier 35:133–141

Isogai T, Yanagisawa M, Isogai A (2009) Degrees of polymerization (DP) and DP distribution of cellouronic acids prepared from alkali-treated celluloses and ball-milled native celluloses by TEMPO-mediated oxidation. Cellulose 16:117–127. doi:10.1007/s10570-008-9245-1

Japas ML, Franck EU (1985) High pressure phase equilibria and PVT-data of the water-oxygen system including water-air to 673 K and 250 MPa. Ber Bunsen-Ges Phys Chem 89:1268–1275. doi:10.1002/bbpc.19850891206

Kabyemela BM, Adschiri T, Malaluan RM, Arai K (1999) Glucose and fructose decomposition in subcritical and supercritical water: detailed reaction pathway, mechanisms, and kinetics. Ind Eng Chem Res 38:2888–2895. doi:10.1021/ie9806390

Kalinichev AG (2001) Molecular simulations of liquid and supercritical water: Thermodynamics, structure, and hydrogen bonding. Rev Mineral Geochem 42:83–129. doi:10.2138/rmg.2001.42.4

Kruse A (2008) Supercritical water gasification. Biofuels Bioprod Biorefin 2:415–437. doi:10.1002/bbb.93

Langan P, Sukumar N, Nishiyama Y, Chanzy H (2005) Synchrotron X-ray structures of cellulose II and regenerated cellulose II at ambient temperature and 100 K. Cellulose 12:551–562. doi:10.1007/s10570-005-9006-3

Larsson PT, Wickholm K, Iversen T (1997) A CP/MAS $^{13}$C NMR investigation of molecular ordering in celluloses. Carbohydr Res 302:19–25. doi:10.1016/S0008-6215(97)00130-4

Lemmon EW, McLinden MO, Friend DG (2013) Thermophysical properties of fluid systems. In: NIST chemistry WebBook. National Institute of Standards and Technology. Available via NIST Standard Reference Database Number 69. http://webbook.nist.gov. Accessed June 13

Leppänen K, Andersson S, Torkkeli M, Knaapila M, Kotelnikova N, Serimaa R (2009) Structure of cellulose and microcrystalline cellulose from various wood species, cotton and flax studied by X-ray scattering. Cellulose 16:999–1015. doi:10.1007/s10570-009-9298-9

Marshall WL, Franck EU (1981) Ion product of water substance, 0–1,000 °C, 1–10,000 bars. New international formulation and its background. J Phys Chem Ref Data 10:295–304. doi:10.1063/1.555643

Newman RH (2008) Simulation of X-ray diffractograms relevant to the purported polymorphs cellulose $IV_I$ and $IV_{II}$. Cellulose 15:769–778. doi:10.1007/s10570-008-9225-5

Parikka M (2004) Global biomass fuel resources. Biomass Bioenerg 27:613–620. doi:10.1016/j.biombioe.2003.07.005

Penttilä PA, Varnai A, Leppänen K, Peura M, Kallonen A, Jääskeläinen P, Lucenius J, Ruokolainen J, Siika-aho M, Viikari L, Serimaa R (2010) Changes in submicrometer structure of enzymatically hydrolyzed microcrystalline cellulose. Biomacromolecules 11:1111–1117. doi:10.1021/bm1001119

Sasaki M, Kabyemela B, Malaluan R, Hirose S, Takeda N, Adschiri T, Arai K (1998) Cellulose hydrolysis in subcritical and supercritical water. J Supercrit Fluids 13:261–268. doi:10.1016/S0896-8446(98)00060-6

Sasaki M, Fang Z, Fukushima Y, Adschiri T, Arai K (2000) Dissolution and hydrolysis of cellulose in subcritical and supercritical water. Ind Eng Chem Res 39:2883–2890. doi:10.1021/ie990690j

Sasaki M, Adschiri T, Arai K (2003) Production of cellulose II from native cellulose by near- and supercritical water solubilization. J Agric Food Chem 51:5376–5381. doi:10.1021/jf025989i

Sasaki M, Adschiri T, Arai K (2004) Kinetics of cellulose conversion at 25 MPa in sub- and supercritical water. AIChE J 50:192–202. doi:10.1002/aic.10018

Schelosky N, Roeder T, Baldinger T (1999) Molecular mass distribution of cellulosic products by size exclusion chromatography in DMAc/LiCl. Papier 53:728–738

Sharples A (1957) The hydrolysis of cellulose and its relation to structure. Trans Faraday Soc 53:1003–1013. doi:10.1039/TF9575301003

Sharples A (1958) The hydrolysis of cellulose and its relation to structure part 2. Trans Faraday Soc 54:913–917. doi:10.1039/TF9585400913

Siegenthaler U, Sarmiento JL (1993) Atmospheric carbon dioxide and the ocean. Nature (London) 365:119–125. doi:10.1038/365119a0

Tolonen LK, Zuckerstatter G, Penttilä PA, Milacher W, Habicht W, Serimaa R, Kruse A, Sixta H (2011) Structural changes in microcrystalline cellulose in subcritical water treatment. Biomacromolecules 12:2544–2551. doi:10.1021/bm200351y

Uematsu M, Franck EU (1980) Static dielectric constant of water and steam. J Phys Chem Ref Data 9:1291–1306. doi:10.1063/1.555632

Wickholm K, Larsson PT, Iversen T (1998) Assignment of noncrystalline forms in cellulose I by CP/MAS $^{13}$C NMR spectroscopy. Carbohydr Res 312:123–129. doi:10.1016/S0008-6215(98)00236-5

Yu Y, Wu H (2009) Characteristics and precipitation of glucose oligomers in the fresh liquid products obtained from the hydrolysis of cellulose in hot-compressed water. Ind Eng Chem Res 48:10682–10690. doi:10.1021/ie900768m

Zuckerstätter G, Schild G, Wollboldt P, Röder T, Weber HK, Sixta H (2009) The elucidation of cellulose supramolecular structure by CP/MAS $^{13}$C NMR. Lenzinger Berichte 87:38–46